Supplementary Information for

Independent blazed diffraction in a polarization insensitive dual waveband metagrating

Xinran Su[1], Pengtao Hu[1], Kai Wu[3,4],Yingge Cong[1] ,Junlin Li[1], Mingfeng Ge[1,*], Xiaoyi Liu[3,4,*], Ruoqian Gao[1,2,*], Wenfei Dong[1]

[1]Department of Biomaterials and Stem Cells,Suzhou Institute of Biomedical Engineering and Technology, Chinese Academy of Science, Suzhou 215163, China

[2]CAS Key Lab of Bio-Medical Diagnostics, Suzhou Institute of Biomedical Engineering and Technology, Chinese Academy of Sciences, Suzhou, Jiangsu 215163, China

[3]School of Optoelectronic Science and Engineering & Collaborative Innovation Center of Suzhou Nano Science and Technology, Soochow University, Suzhou 215006, China;

[4]Key Lab of Advanced Optical Manufacturing Technologies of Jiangsu Province & Key Lab of Modern Optical Technologies of Education Ministry of China, Soochow University, Suzhou 215006, China;

[*]Corresponding email: gemf@sibet.ac.cn;xyliu@suda.edu.cn; gaorq@sibet.ac.cn;

Table S1. Dimensions and phase responses of the single-blaze unit sequence in the 620 ‑ 660 nm band (H = 800 nm).

Nanostructure index	r(nm)	λ=620 nm	λ=630 nm	λ=640 nm	λ=650 nm	λ=660 nm
1	61.9	0°	31.2597°	46.302°	22.0521°	77.4072°
2	76.76	35.9601°	69.1628°	118.1691°	93.5114°	108.8111°
3	130	81.7119°	156.4981°	194.525°	165°	176.3697°
4	141.6	197.667°	250.633°	233.8696°	237°	248.8259°
5	147	316.5585°	311.6632°	343.53°	309°	350.0039°

Table S2. Dimensions and phase responses of the single-blaze unit sequence in the 970 ‑ 1010 nm band (H = 800 nm).

Nanostructure index	r(nm)	λ=970 nm	λ=980 nm	λ=990 nm	λ=1000 nm	λ=1010 nm
1	63.33	60.1168°	40.157°	6.154°	43.181°	24.1333°
2	90	106.3453°	85.5187°	66.886°	115.614°	108.808°
3	98.2	141.1897°	133.9016°	126.762°	173.0303°	162.794°
4	103.5	209.951°	197.702°	186.301°	224.1233°	208.6855°
5	108.6	285.2381°	264.855°	246.34°	278.65°	258.3289°
6	120	353.4674°	329.4256°	306.4688°	332.9712°	310.9647°

Table S3. Dimensions and phase responses of the hybrid-blaze unit sequence in the 620–660 nm band (H = 780 nm).

Nanostructure index	r(nm)	λ=620 nm	λ=630 nm	λ=640 nm	λ=650 nm	λ=660 nm
1	61.9	69.71741°	24.9274°	340.4415°	305.1853°	262.7027°
2	76.67	89.06392°	66.30462°	43.04622°	17.90872°	12.90287°
3	130	192.1606°	144.1635°	114.5581°	94.67106°	89.50201°
4	141.6	302.0573°	238.7997°	213.9729°	147.2106°	120.6425°
5	147	29.42469°	276.242°	309.927°	236.7008°	174.6235°

Table S4. Dimensions and phase responses of the hybrid-blaze unit sequence in the 970–1010 nm band (H = 780 nm).

Nanostructure index	r(nm)	λ=970 nm	λ=980 nm	λ=990 nm	λ=1000 nm	λ=1010 nm
1	63.33	140.2175°	132.9331°	125.8109°	120.0452°	113.1918°
2	90	207.1911°	195.1463°	183.9054°	175.9214°	165.7988°
3	98.2	279.6849°	259.8009°	241.6581°	225.1005°	210.0179°
4	103.5	346.3668°	322.7723°	300.1751°	277.9022°	257.9713°
5	108.6	81.16088°	23.6694°	357.0637°	331.1592°	309.5826°
6	120	97.27081°	79.26141°	62.14247°	44.79366°	26.29841°

Table S5. Dimensions and phase responses of the partial-blaze unit sequence in the 620–660 nm band (H = 800 nm).

Nanostructure index	r(nm)	λ=620 nm	λ=630 nm	λ=640 nm	λ=650 nm	λ=660 nm
1	70	66.1648°	35.7063°	25.2483°	0.61143°	325.3217°
2	80	89.8646°	66.3015°	57.093°	34.6602°	12.2611°
3	130	197.667°	156.4981°	118.1691°	93.5114°	77.4072°
4	135	241.171°	187.0785°	144.8959°	108.3921°	85.321°
5	142	323.6365°	250.5149°	198.6703°	171.6745°	113.8808°

Table S6. Dimensions and phase responses of the partial-blaze unit sequence in the 970–1010 nm band (H = 800 nm).

Nanostructure index	r(nm)	λ=970 nm	λ=980 nm	λ=990 nm	λ=1000 nm	λ=1010 nm
1	50	130.4151°	123.4187°	116.5543°	104.4257°	97.9097°
2	60.1	138.1499°	130.9597°	123.9135°	112.461°	105.7534°
3	70.2	150.6328°	142.978°	135.4985°	122.566°	115.5068°
4	80.3	172.017°	163.1149°	154.5608°	139.8976°	132.0638°
5	90.4	212.3786°	199.8672°	188.3057°	174.6547°	164.2591°
6	100.5	316.3884°	293.6855°	272.6523°	248.8394°	230.8977°

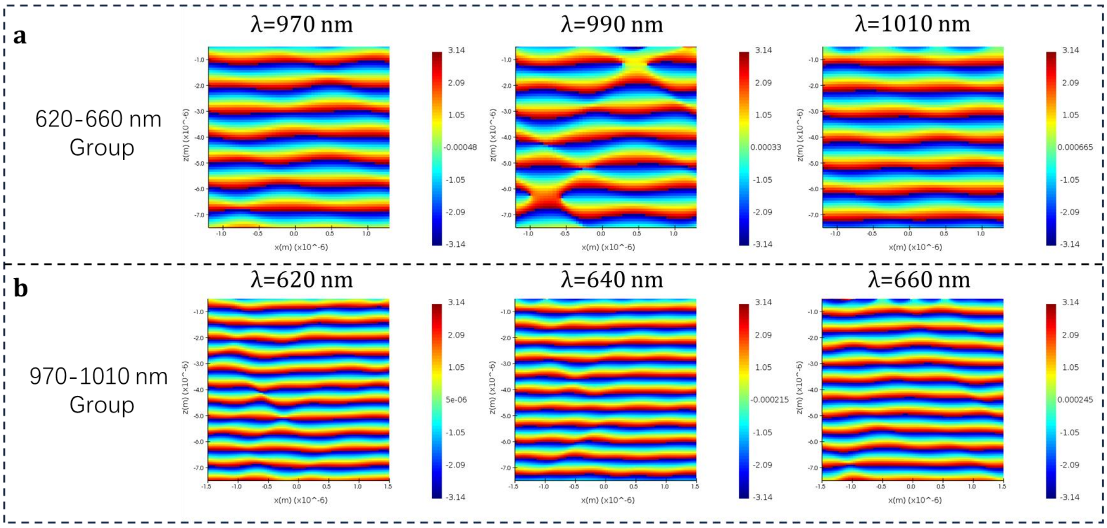

Fig. S1 Phase responses of the two meta-unit groups in the opposite operating band under the single-blaze mode. In the non-target band, each group shows an almost flat transmission phase. It therefore serves as a phase-background group in the overall modulation.(a) Transmission phase of the visible-band unit group (620–660 nm) evaluated in the near-infrared band (970–1010 nm). The phase stays nearly constant across the band, indicating a background-phase role.(b) Transmission phase of the near-infrared unit group (970–1010 nm) evaluated in the visible band (620–660 nm). The phase is also nearly flat, and the unit group acts as a phase background in the non-design band.

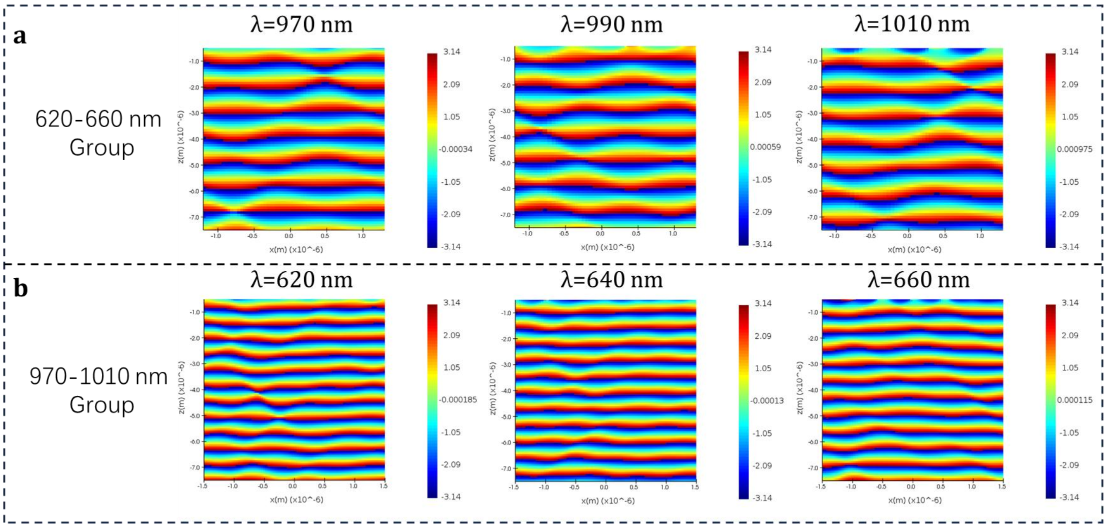

Fig. S2 Phase responses of the two meta-unit groups in the opposite operating band under the hybrid-blaze mode. In the non-target band, both unit groups exhibit an almost flat transmission phase. They therefore act as phase-background groups in the overall modulation.(a) Transmission phase of the visible-band unit group (620–660 nm) evaluated in the near-infrared band (970–1010 nm). The phase remains nearly constant, indicating a background-phase contribution.(b) Transmission phase of the near-infrared unit group (970–1010 nm) evaluated in the visible band (620–660 nm). A similar flat phase response is observed, and the unit group serves as a phase background in the non-design band.

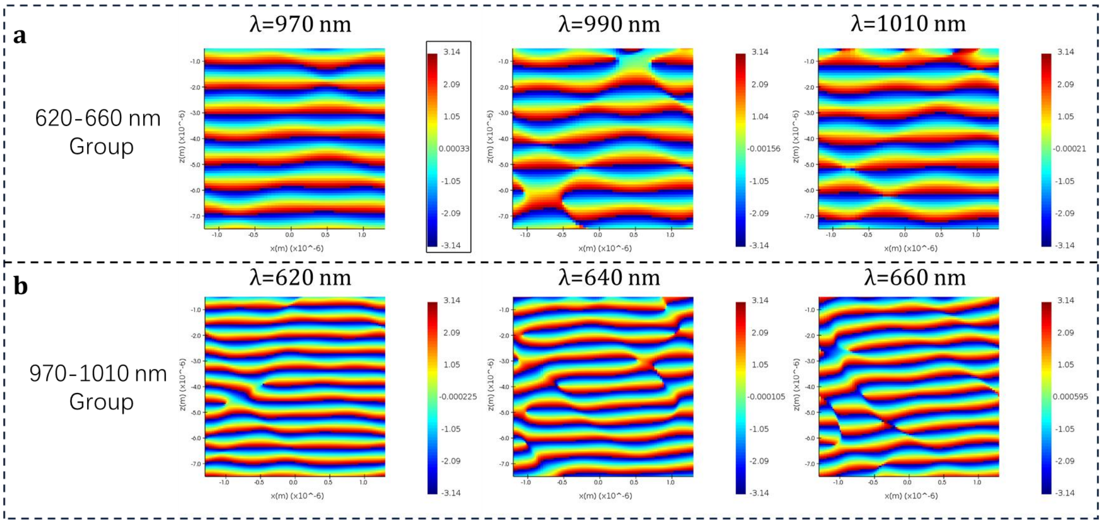

Fig. S3 Phase responses of the two meta-unit groups in the opposite operating band under the partial-blaze mode. In the non-target band, both unit groups show an almost flat transmission phase. They therefore act as phase-background groups in the overall modulation.(a) Transmission phase of the visible-band unit group (620–660 nm) evaluated in the near-infrared band (970–1010 nm). The phase is nearly constant across the band, indicating a background-phase contribution.(b) Transmission phase of the near-infrared unit group (970–1010 nm) evaluated in the visible band (620–660 nm). The phase remains almost flat, and the unit group serves as a phase background in the non-design band.

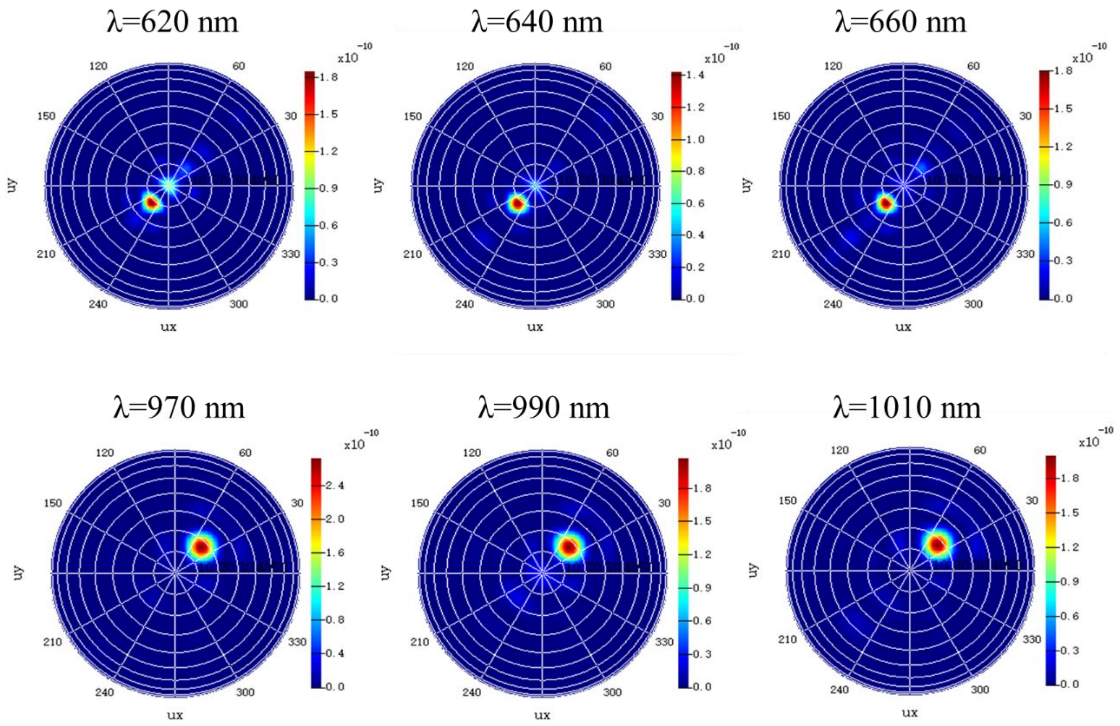
λ=620 nm
λ=640 nm
λ=660 nm
λ=970 nm
λ=990 nm
λ=1010 nm

Fig. S4 Transmitted far-field intensity distributions of the dual-band single-blaze metagrating at the operating wavelength ranges of 620–660 nm and 970–1010 nm.

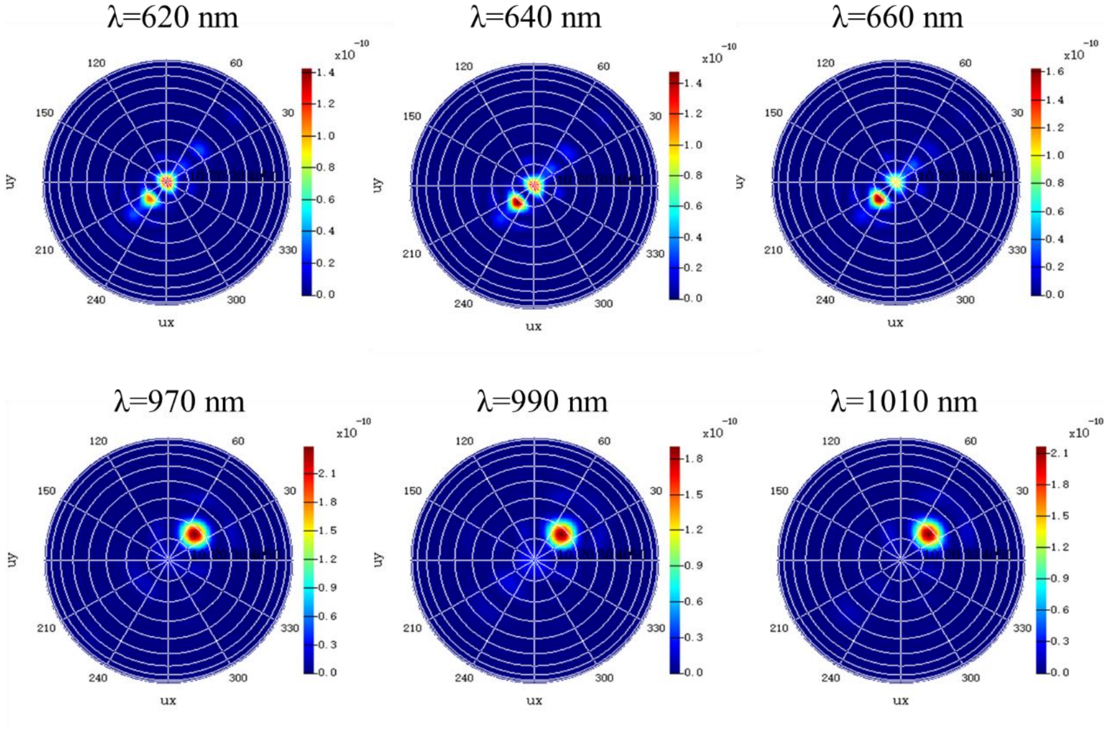

Fig. S5 Transmitted far-field intensity distributions of the dual-band hybrid-blaze metagrating at the operating wavelength ranges of 620–660 nm and 970–1010 nm.

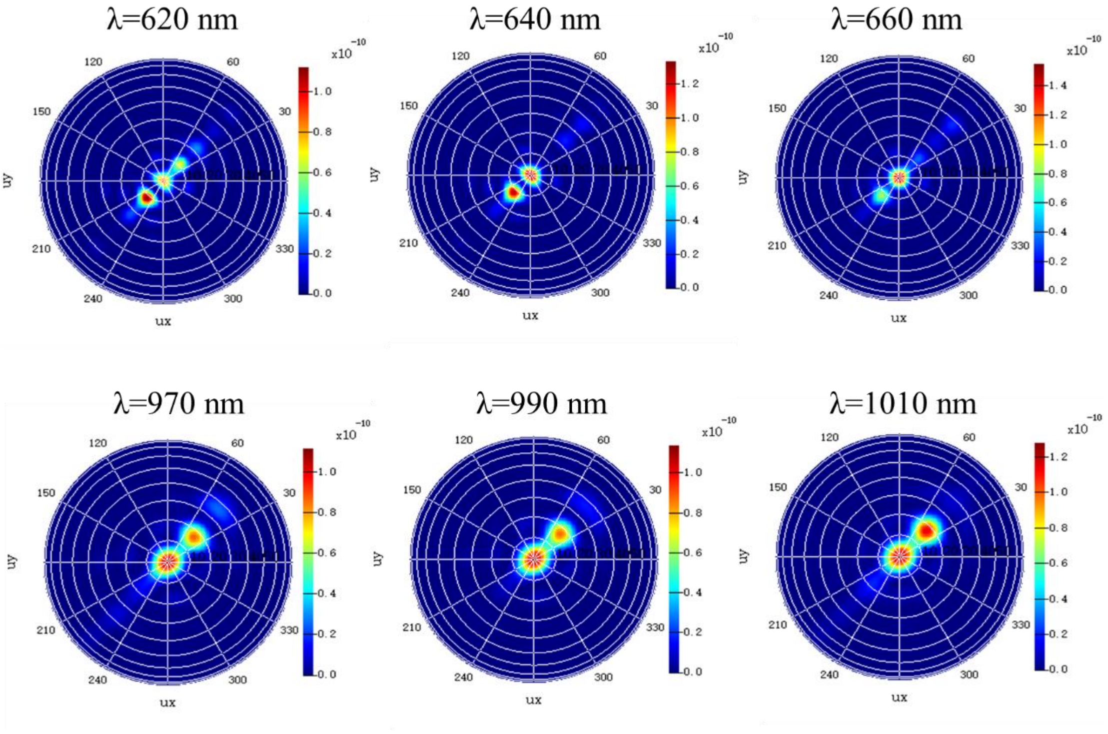

Fig. S6 Transmitted far-field intensity distributions of the dual-band partial-blaze metagrating at the operating wavelength ranges of 620–660 nm and 970–1010 nm.

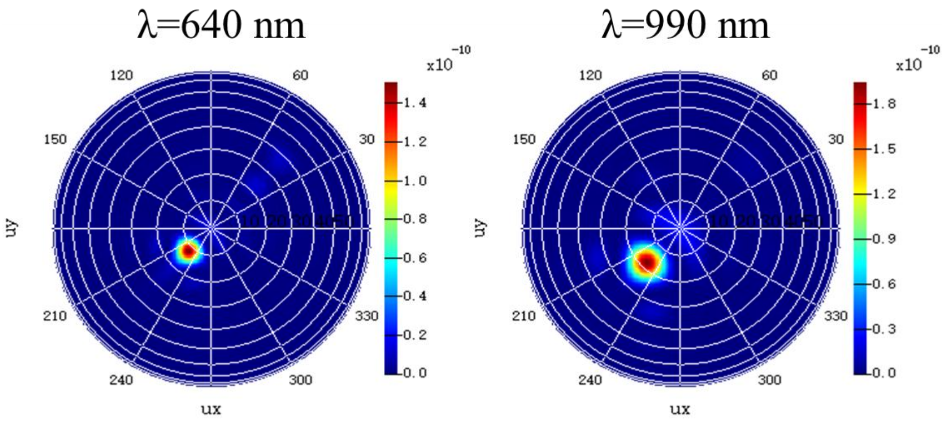

Fig. S7. Dual-band same-order single-blaze design, where the transmitted energy is directed into the −1st diffraction order at both λ = 640 nm and λ = 990 nm.

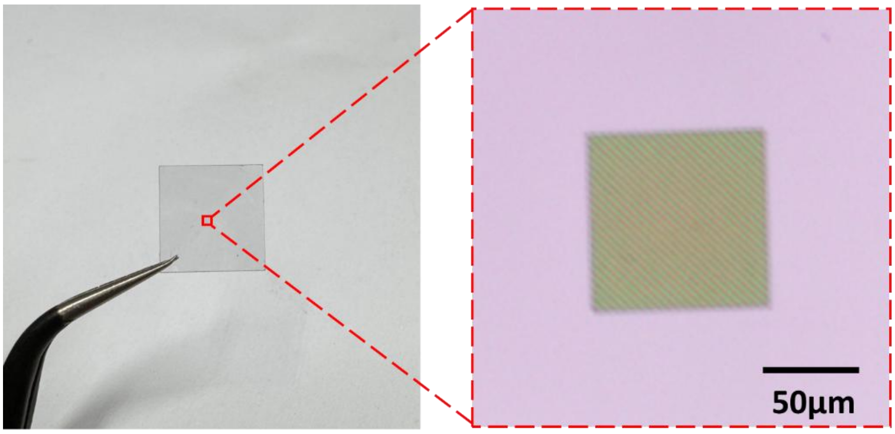

Fig. S8 Images of the proposed metagrating. The left panel shows a macroscopic photograph of the metagrating fabricated on a sapphire substrate. The right panel shows an optical microscope image of the overall structural outline.

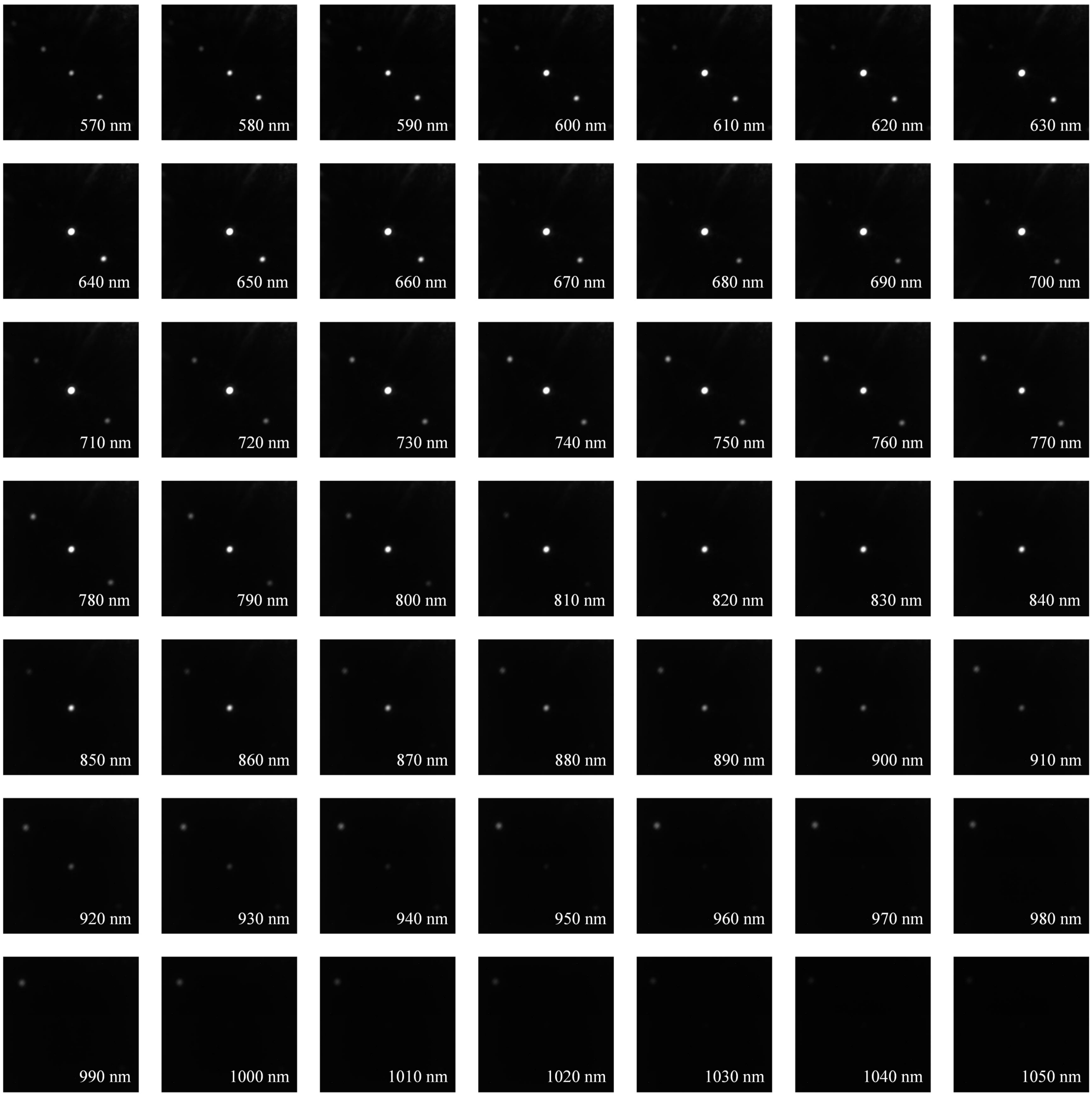

Fig. S9 Two-dimensional diffraction patterns measured across the 570–1050 nm spectral range.

Supplementary Equation

The theoretical calculation is based on the general form of the grating equation：

$$n_t \sin\theta_m = \mathrm{m}\frac{\lambda_0}{d} \tag{S1}$$

Here, the transmission-side medium is sapphire, with a refractive index of $n_t \approx 1.75$. Because the device adopts a staggered interleaved layout, two adjacent units with a period of 400 nm jointly form a supercell along the phase-gradient direction. The corresponding effective grating period can be written as $d = (400 + 400) \times \sqrt{2}$. Based on this relation, the diffraction angles $\theta_m$at different wavelengths are calculated, and the corresponding values of $\tan\theta_m$are then obtained. In the experimental setup, the lateral displacement of the far-field diffraction spots satisfies the geometric relation $\Delta x \propto \tan\theta_m$. Therefore, the experimentally measured spot displacement can be directly compared with the calculated values of $\tan\theta_m$.